A national laboratory of the U.S. Department of Energy
Office of Energy Efficiency & Renewable Energy

National Renewable Energy Laboratory

Innovation for Our Energy Future

Degradation of ZnO Window Layer for CIGS by Damp-Heat Exposure

Preprint

F.J. Pern, B. To, C. DeHart, X. Li, and S.H. Glick
National Renewable Energy Laboratory

R. Noufi
SoloPower, Inc.

To be presented at 2008 SPIE PV Reliability Symposium
San Diego, California
August 10–14, 2008

Conference Paper
NREL/CP-520-42792
August 2008

NREL is operated by Midwest Research Institute • Battelle Contract No. DE-AC36-99-GO10337

Degradation of ZnO-based window layers for thin-film CIGS by accelerated stress exposures

F. J. Pern, R. Noufi[1], B. To, C. DeHart, X. Li, and S. H. Glick

National Center for Photovoltaics (NCPV)
National Renewable Energy Laboratory (NREL)
1617 Cole Blvd., Golden, CO 80401
[1] SoloPower Inc., 5981 Optical Court, San Jose, CA 95138

ABSTRACT

The reliability of ZnO-based window layer for $CuInGaSe_2$ (CIGS) solar cells was investigated. Samples of RF magnetron-sputtered, single-layer intrinsic and Al-doped ZnO and their combined bilayer on glass substrates were exposed in a weatherometer (WOM) and damp heat (DH) conditions with or without acetic acid vapor. Some preliminary samples of single-layer Al-doped $Zn_{1-x}Mg_xO$ (ZMO) alloy, a potential replacement for Al:ZnO with a wider bandgap, were also evaluated in the DH. The Al-doped ZnO and ZMO films showed irreversible loss in the conducting properties, free carrier mobility, and characteristic absorption band feature after <500-h DH exposure, with the originally clear transparent films turned into white hazy insulating films and the degradation rate follows the trend of (DH + acetic acid) > DH > WOM. The degradation rate was also reduced by higher film thickness, higher deposition substrate temperature, and dry-out intervals. The results of X-ray diffraction analysis indicate that the ZnO-based films underwent structural degeneration by losing their highly (002) preferential orientation with possible transformation from hexagonal into cubic and formation of $Zn(OH)_2$. Periodic optical micro-imaging observations suggested a temporal process that involves initial hydrolysis of the oxides at sporadic weak spots, swelling and popping of the hydrolyzed spots due to volume increase, segregation of hydrolyzed regions causing discontinuity of electrical path, hydrolysis of the oxide-glass interface, and finally, formation of insulating oxides/hydroxides with visible delamination over larger areas.

Key words: transparent conducting oxides, intrinsic and Al-doped ZnO, ZnMgO alloy, accelerated exposure, damp heat, weatherometer, degradation, CIGS, thin-film solar cell.

INTRODUCTION

Advancements in thin-film PV technologies coupled with a tight shortage of crystalline Si in the past years have enabled their market acceptance with a share of 10.4% in 2008, in which the amorphous and micromorph Si products take up 5.2%, CdTe 4.7% with a large gain last year, and a small 0.5% for $CuInGaSe_2$ (CIGS).[1] In the device construction of thin-film PV technologies, essentially all require the use of at least one transparent conducting oxide (TCO) as a contact electrode. Minami and Fortunato et al. reviewed and discussed the properties, requirements, and/or material design of various TCOs, including indium tin oxide (ITO), ZnO, and SnO_2 for PV applications, and Gordon discussed the criteria for choosing the TCOs for different applications.[2-4] Among a variety of TCOs, thin-film ZnO doped with different metals have been widely used as contact electrodes in thin-film PV technologies such as a-Si, micromorph Si, and $CuIn_{1-x}(Ga)_xSe_2$ (CIS or CIGS).[3,5-7] ZnO is also used as an interlayer between the a-Si and microcrystalline Si in the micromorph Si solar cells,[8] and antireflection coating for spherical Si solar cells.[9] ZnO nanowires are also being investigated as charge transport media in nano-hybrid polymer,[3] dye-sensitized,[10] and core/shell structured solar cells.[11]

Most of the present CIS- or CIGS-based PV modules employ ZnO as the conducting front contact electrodes, except for Global Solar, which uses ITO.[12] The bilayer ZnO window layers are typically constructed with an intrinsic ZnO over the CdS layer, followed by an Al-doped ZnO. The intrinsic ZnO serves as a buffer layer that is believed to enhance the performance and thermal stability as reasoned by Roedern.[13] The optical and electrical properties of ZnO, doped and

undoped, are strongly affected by its defect chemistry, as reviewed by Schmidt-Mende and MacManus-Driscoll for nanostructures and device applications.[14]

At NREL, bilayer ZnO has been used on high-efficiency CIGS solar cells for years because of its high optical transmittance and low fabrication temperature; a new world record efficiency of 19.9% was recently reported by Repins et al.[15] Recently, intrinsic and Al-doped $Zn_{1-x}Mg_xO$ (ZMO) alloys have been investigated for potential replacement of the ZnO based on their tunable wider-bandgap engineering to gain some current in the short-wavelength range and better conduction-band edge matching to minimize a conduction-band offset between ZnO and CIGS, which reduces the cell's open-circuit voltage.[16,17] These improvements in the short-circuit current density (J_{sc}) and V_{oc} may also improve the fill factor (FF) and hence the CIGS cell efficiency. The band structure of ZnO can be engineered by alloying with MgO to form new compounds with appropriate optical and electronic properties.[18,19] A concern of this approach is the stability of the alloys, as Ryoken et al. reported,[20] that high concentration of Al in ZnO and Mg in $Zn_{1-x}Mg_xO$ alloys introduces non-equilibrium defects into ZnO films that are the cause of crystallinity degradation and thermal instability.

As discussed above, ZnO-based contact electrodes and materials are widely used for PV devices (and other applications). Therefore, along with the Mo base electrode, their stability can become a critical determining factor in the long-term performance reliability of the PV module, which requires not only reliable constituent component materials and device structure of the solar cells, but also reliable electrical interconnects and packaging. Currently, to assess the quality of a PV module, one of the qualification tests in the IEC61215 or IEC61464 specifies a 1000-h exposure in damp heat (DH) at 85^{o}C and 85% relative humidity (RH). Passing the damp heat test is generally agreed to be the number one concern, especially for thin-film PV modules. As recently presented by Whitfield, there was a 42% failure by the DH exposure followed by a 40% failure by 200 thermal cycles in IEC 61215 qualification tests (for c-Si modules) conducted at TÜV Rheinland since 1998 and a ~28% failure by DH followed by 14% outdoors for thin-film technologies conducted at ASU-PTL between 1997 and 2005.[21] Accordingly, a systematic evaluation of the performance reliability of ZnO as well as other TCOs is essential, not only to assess the material stability, but also to address the need for improvements by implementing effective mitigation methods or seeking more reliable new/replacement materials, and to develop reliable packaging technology.

We have conducted stability studies for the Mo base electrode on soda lime glass and a number of instrinsic ZnO and Al-doped ZnO and $Zn_{1-x}Mg_xO$ alloys using accelerated stress tests that include DH with and without acetic acid, dry heat, and in a weatherometer. The results showing the severe degradation of Mo and ZnO in DH have been reported in two separate meetings.[22,23] There are also some earlier reports on the stability issues of Al:ZnO by DH exposure in the literature.[24-26] Lin and coworkers reported their observations of a greater electrical degradation for thinner Al:ZnO thin films sputtered on glass, but little change in optical transmittance measured in 300-800 nm range.[27] Recently, Wiedeman et al. at Global Solar reported high stability of their *rigid* CIGS products in >3000-h DH exposure, but notable degradation for flexible package after ~550 h.[28] Feist et al. reported a >50% efficiency loss for encapsulated CIGSS on soda lime glass from Shell Solar after 168 h of 85^{o}C/100%RH exposure and that the degradation of Al-doped ZnO could be the lifetime-limiting factor.[29] In an effort to mitigate the DH attack on CIGS from Shell Solar (with Al:ZnO) and IEC (with ITO), Olson and coworkers demonstrated the efficacy of a multi-layer, transparent moisture barrier coating with varying degree of success that was dependent on the TCO type, roughness of CIGS, and encapsulation.[30,31] Very recently, Vitex Systems reported that the flexible CIGS solar cells encapsulated with their multilayer "flexible glass" retained 98% of their original efficiency after 1100 h exposure in DH.[32] It is not clear if the two groups used the same multilayer technology, however. Using a simple coating with PMMA, Kim et al. found the polymer coating was useful in blocking moisture and air to reduce the degradation of ZnO nanowire devices.[33]

This paper summarizes our work with more details and an emphasis on the DH-induced degradation of Al-doped ZnO and $Zn_{1-x}Mg_xO$ alloys. The other two TCOs, ITO and F:SnO_2, are not included here.[23] It should be noted that these studies, which allowed the bare ZNO-based coatings on the glass substrates to be exposed directly to the accelerated stress/weathering conditions, represent a fairly extreme situation that normally may not be experienced by a well-encapsulated and packaged PV module. Accordingly, these studies represent primarily our efforts to evaluate and compare the stability of various ZnO materials for thin-film CIGS PV applications.

EXPERIMENTAL

Two experiments were conducted. In the first experiment, which was more exploratory in nature to establish/define the methodology and procedures for accelerated life tests, the bilayer i-/Al:ZnO samples were old "witness" films deposited along with CIGS solar cells in a Semicore/MRC603 system on thin 0.5-mm 7059 glass slides with some variations in films' structural quality as observed in XRD. In the second experiment, consistent ZnO film overall quality was ensured as described in (a) below.

(a) TCO samples. Two RF magnetron sputtering systems were used to prepare ZnO samples separately. On a Semicore/MRC603 system, ~0.1-μm single-layer intrinsic ZnO (IZO) and Al-doped ZnO (AZO), and ~0.2-μm bi-layer ZnO (BZO), were prepared on 7.6-cm x 7.6-cm x 1.1-mm 7059 glass plates. The IZO was made from a 99.99% pure ZnO target in a 5- mTorr deposition chamber pressure and a flow rate of 60 sccm of Ar with 1% O_2 by using ~1 watt/cm^2 RF power density. For AZO deposition, the target was a 99.99% ZnO with 2 wt% Al_2O_3 using a ~1.2 watts/cm^2 RF power density in Ar at a flow rate of 40 sccm. The *in-situ* substrate temperatures were determined to not exceed 60^{o}C with a temperature indicator strip. During the sputtering deposition, the substrate holder platform was translated ("scanned") back and forth in front of the target at a rate of 25 cm/min. An ATC 2200-V sputtering system from AJA International, Inc., was employed to prepare the sample set of single-layer, Al-doped ZnO with or without MgO (Al:$Zn_{1-x}Mg_xO$, x= 0 to 0.33; ZMO), at a thickness of 0.3~0.6 μm. The ATC 2200-V system has the ability to co-sputter, where the vacuum system base pressure was typically maintained at 2 x 10^{-8} Torr. A rotatable substrate station is positioned over the two 3"-diameter targets that are tilted toward the substrate and positioned in line with each other, as recently described by Li and co-workers.[16] The ZnO target was 99.999% pure with 98 wt% ZnO and 2 wt% Al_2O_3 (1.56 at% Al) and the MgO target was 99.95% pure, and both were used as received from Cerac Inc. The Al:$Zn_{1-x}Mg_xO$ (ZMO) films were sputtered on 6" x 6" 1737 Corning glass at a working pressure of 5 mTorr in Ar at a flow rate of 40 sccm. The RF power varied between 60 and 240 watts, depending on the desired Mg content and deposition rate. The substrate temperature could deviate somewhat from the programmed temperature as a result of ~1-cm gap between the substrate and the monitoring thermocouple.

(b) Accelerated exposure tests (AET). In the first experiment, only BZO samples were studied and were exposed separately in (i) a Blue M environmental chamber that operated at the "damp heat" (DH) test condition of 85^{o}C and 85% RH; (ii) an Atlas Ci4000 weatherometer (WOM) chamber, running at 2.5 UV-sun, 60^{o}C, and 60% RH; or (iii) an oven set at 85^{o}C with samples placed in glass jars in which the RH level was controlled at 78% by saturated KCl with or without a small amount of glacier acetic acid (0.1 mL in a 250 mL jar). In the second experiment, all ZnO and ZMO samples were exposed only in the DH chamber.[22,23]

(c) Chemical and physical mitigations. Two preliminary studies were conducted. Some of the BZO samples in the first experiments were treated briefly in a diluted solution of a special polydimethylsiloxane (PDMS) to investigate the usefulness of the chemical treatment to stabilize the ZnO against DH by increasing hydrophobicity.[22] In the physical mitigation approach, a thin layer (~0.4 ± 0.2 μm) of SiO_xN_y was PECVD-deposited on the BZO as moisture barrier.[34]

(d) Analytical characterization. Specimens of ~2.0 cm x 2.8 cm were cut from the ZnO-coated plates for the convenience of testing and various measurements. After baseline measurements, the samples were characterized periodically during the course of DH exposure. Transmittance and reflectance measurements for optical properties were conducted on a Cary 5G or 6000i UV-Vis-NIR spectrophotometer with an integration sphere. Hall measurements were performed on an Ascent Hall550 Advance system for sheet resistance (R□), free-carrier mobility, and concentration. An X1 Advanced Diffraction System from Scintag, Inc. was used for the x-ray diffraction (XRD) analysis for structural changes. Interference optical micro-imaging for morphological changes were obtained on a WYKO Optical Profiler Model 1100 system from Veeco. Upon completion of the experiments, the exposed samples were examined with scanning electron microscopy (SEM) on a Nova Nano SEM 630 system from FEI.

RESULTS AND DISCUSSIONS

The results will be divided into several sections below to separately discuss degradation of ZnO-based thin films with regard to the optical, electrical, mechanical, and morphological properties.

I. Optical Property and Degradation

The ZnO-based thin films exhibited different transmittance and reflectance spectra depending primarily on their carrier concentration and film thickness. Figure 1a shows the transmittance spectra for the Semicore-deposited IZO, AZO, and BZO. Doping with Al in AZO produced the free-carrier absorption band at >1000 nm. When the IZO and AZO were combined to BZO bilayer, which showed a bandgap of 3.3-3.4 eV, greater free-carrier absorption band and optical effect were observed as seen in Fig. 1a. The effects were more obvious when the film was thicker and R□ lower, as shown in Fig. 1b where the CIGS bandgap was also marked.[35] As a note, NREL's CIGS solar cell devices normally use the ~0.2-µm BZO. The transmittance and reflectance spectra for three Al:$Zn_{1-x}Mg_xO$ (x = 0, 0.01, 0.1) ZMO films prepared on the ATC 2200-V sputtering system are given in Fig. 2. At 0.3 and 0.5 µm thick, the optical effect of interference patterns appeared, similar to those shown in Fig. 1b.

Figure 3 illustrates the observed optical changes for some of the samples subjected to the three AET conditions. The BZO films that were in the first experiment showed that the degrading effect was the least for WOM exposure (Fig. 3a) and the greatest for DH exposure in the presence of acetic acid vapor (Fig. 3b).[22] The acetic acid was intentionally introduced to simulate the possible presence of the acid from thermal processing and photothermal degradation of the ethylene-vinyl acetate (EVA) encapsulant commonly used in PV module encapsulation.[36] Its presence in DH likely accelerated or facilitated the hydrolysis of ZnO into $Zn(OH)_2$. When exposed in DH without acetic acid vapor, all of the ZnO and ZMO samples turned from initially clear into hazy white and became highly resistive after 480 h, and their transmittance and reflectance spectra became flat and almost identical (Figs. 3c-3f). The originally conductive ZnO (AZO and BZO) and ZMO films also lost their characteristic free-carrier absorption tail bands.[23]

II. Electrical Property and Degradation

The typical sheet resistance (R□) as determined from Hall measurements was high at $>10^6$ ohm/sq for the IZO, ~85 ohm/sq for AZO at ~0.1 µm, and 65~75 ohm/sq for BZO at ~0.2 µm. For the Al:$Zn_{1-x}Mg_xO$ (x = 0, 0.01, 0.1) ZMO films prepared on the ATC 2200-V sputtering system, the film at x = 0 was the same as a single-layer AZO, the ZMO film at x = 0.01 showed a R□ of ~70 ohm/sq, and the ZMO film became highly resistive at x = 0.1. Table 1 lists the information of the two sample sets used in the two experiments (top half for the first experiment and bottom

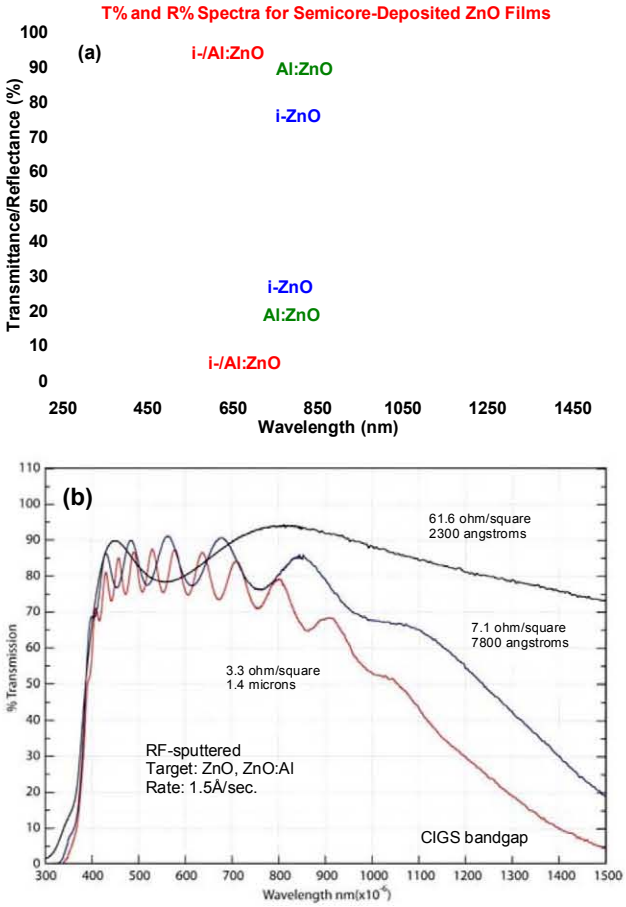

Fig. 1. Transmittance and reflectance spectra for (a) single-layer intrinsic, Al-doped, and bilayer intrinsic/Al-doped ZnO (i-ZnO, Al:ZnO, and i-/Al:ZnO) on glass plates, and (b) three bilayer i-/Al-ZnO films of different sheet resistance and thickness.[35]

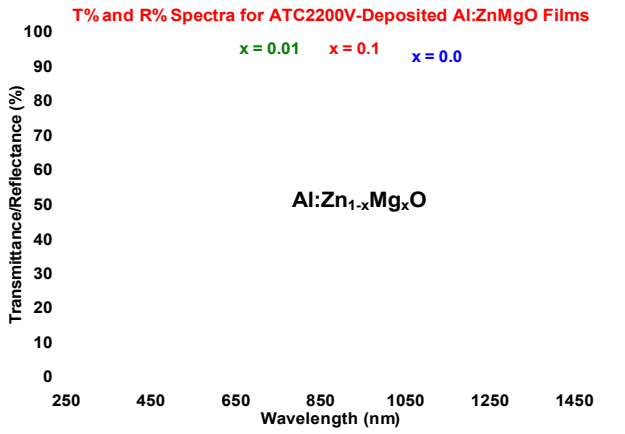

Fig. 2. Transmittance and reflectance spectra for Al-doped $Zn_{1-x}Mg_xO$ films (x = 0, 0.01, and 0.1) sputter-deposited on 1-mm-thick glass plates.

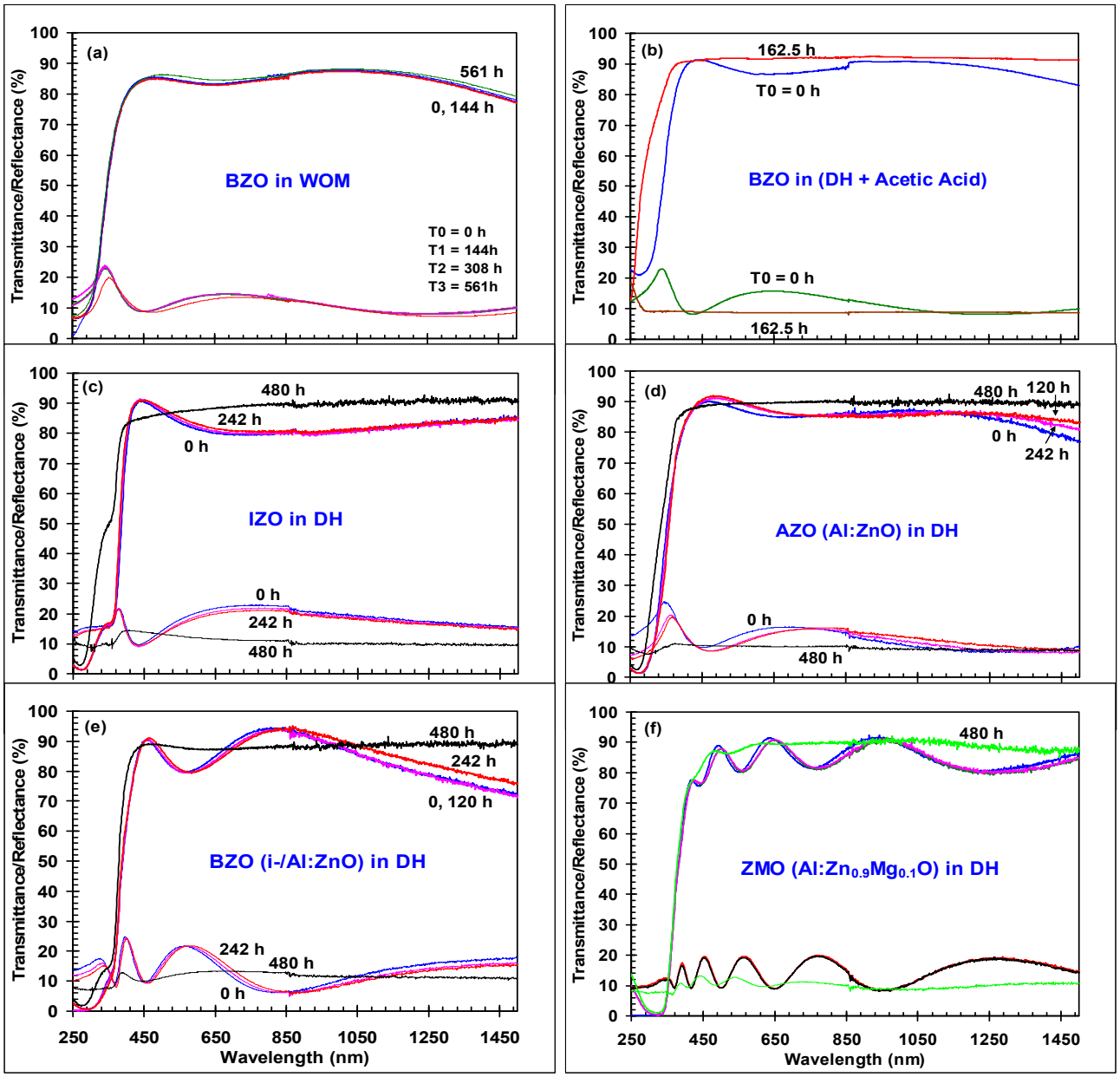

Fig. 3. Transmittance and reflectance spectra for various ZnO and ZMO films on glass upon accelerated exposure tests: (a) in the weatherometer, (b) in damp heat with acetic acid vapor, and (c-f) in damp heat.

Table 1. Sample Data and Degradation Rates upon Accelerated Exposures

Sample ID	BZO-1A	BZO-1B	BZO-1C	BZO-2A	BZO-2B	IZO-11	AZO-21	BZO-31	ZMO-383	ZMO-471	ZMO-501	ZMO-681
Composition	**i-/Al:ZnO**	**i-/Al:ZnO**	**i-/Al:ZnO**	**i-/Al:ZnO**	**i-/Al:ZnO**	**int.-ZnO**	**Al:ZnO**	**i-/Al:ZnO**	**Al:ZnO**	**Al:ZnO**	**Al:ZnO**	**Al:ZnO**
MgO (% wt)										1	10	
Dep. Tsub (oC)	Ambient	Ambient	Ambient	Ambient	Ambient	Ambient	Ambient	Ambient	Ambient	100	100	100
Thickness (µm)	0.2	0.2	0.2	0.2	0.2	0.1	0.1	0.2	0.3	0.5	0.5	0.6
Chem. Mitigation			PDMS	PDMS								
AET Type	DH	DH	DH	DH	WOM	DH	DH	DH	DH	DH	DH	DH
Degrad. Rate [(ohm/sq)/h]	**5.42**	**6.38**	**2.27**	**0.16**	**0.08**	HR* at 0 h	**62.08**	**1.84**	**0.69**	**0.82**	HR* at 0 h	**0.09**

* HR: highly resistive

half for the second experiment) and their degradation rates upon accelerated exposures, mostly in DH and one in the WOM. The actual data of sheet resistance for the second experiment samples were given in ref. 23. The two samples treated briefly with PDMS were also indicated. By assuming a linear degradation, which appeared be valid as shown in Fig. 4 for most samples before they became highly resistive, their degradation rates were calculated and given at the bottom line of Table 1. The samples that were rapidly degraded in DH in the presence of acetic acid vapor (see Fig. 3b) are not tabulated here.

The results indicate that degradation rates of the BZO made by the Semicore/MRC603 system follow the trend of (DH + acetic acid) > DH > WOM, in parallel to the optical results (Fig. 3a). Three significant observations are made here in DH-induced degradation:

1. Thickness effect: thicker Al-doped ZnO or ZMO films degraded more slowly than thinner ones.
2. Substrate-temperature effect: Al-doped ZnO or ZMO films made at higher substrate temperature degraded more slowly than those made at ambient temperature.
3. "Dry-out" effect: Al-doped ZnO films with periodic removal from the DH chamber for measurements degraded more slowly than the specimens (not given in Table 1) exposed in the DH chamber continuously for 240 h.

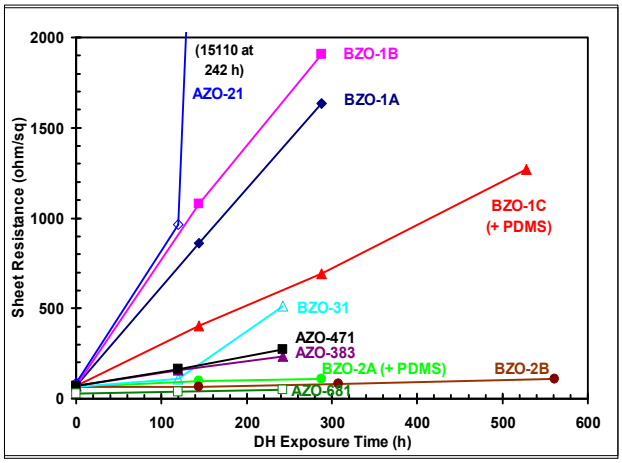

Fig. 4. Sheet resistance changes for the samples in Table 1 as a function of accelerated exposure time before the films became highly resistive

The thickness effect suggests that DH-induced degradation more likely started from the surface of the ZnO or ZMO films and gradually deepened into the bulk and finally to the oxide/glass interfaces. Lin et al. also observed similar thickness effect for their Al:ZnO thin films from 95 nm to 320 nm thick upon DH exposure, and explained it by the larger grain size on the thicker film.[27] The substrate-temperature effect suggests that a better grain crystallite of ZnO or ZMO produced at higher temperature may be more resistant to DH attack. This reasoning appears to be validated by a brief experiment, which resulted in a lower sheet resistance change percentage (28%) for a BZO post-annealed at 200°-220°C for 15 min in a quartz tube in Ar flow than that for an un-annealed specimen (40%) after 94.5 h of DH. The brief annealing increased the BZO specimen's R□ from an original 64 ohm/sq to 83 ohm/sq. More systematic study is required to fully explore the beneficial effect of slower DH-induced degradation for better crystallites made at higher temperature. The "dry-out" effect suggests that the films were capable of recovering their physical properties to some extent after being removed from the DH chamber, as also indicated by the gradual change to a somewhat less cloudy appearance after ~2 days in the air. One likely reason is the loss of water molecules from the hydrated or hydrolyzed film bulk and film/glass interface. A transient effect was noted on a BZO film that was highly resistive when it was still moist just after being taken out from a bottle filled with moisture in the DH chamber, but became conducting as expected for a film with DH = 94 h exposure after drying naturally in the air for some minutes. For those BZO films pretreated with the PDMS, the preliminary results indicate the hydrophobic surface treatment substantially reduced the DH-induced degradation rate (BZO-1C vs. BZO-1A and 1B in Table 1). This is not surprising because a hydrophobic surface, and perhaps also in the grain boundary, of the ZnO would be able to reduce the water molecules from attaching to the ZnO to initiate the subsequent hydration/hydrolysis reaction of degradation.

Along with the increase in the sheet resistance, the ZnO and ZMO films also showed a decrease in mobility, as seen in Fig. 5 (a and b). Consistent with the order in sheet resistance degradation, thicker Al-doped ZnO films in general showed slower loss in mobility (Fig. 5b). Although PDMS treatment was able to reduce the degradation rate in sheet resistance, the mobility of those films exposed in DH decreased essentially the same as for the untreated, suggesting the current PDMS treatment was still inadequate in that moisture still could penetrate and impede the free-carrier movement. On the other hand, the free-carrier concentrations in most of the exposed films showed various degrees of decrease, as illustrated in Fig. 5 (c and d). However, a few samples exhibited an increase, such as DH-exposed Al:$Zn_{0.99}Mg_{0.01}O$ (ZMO-471) and PDMS-treated BZO-1C, and WOM-exposed BZO-2B. The cause for such an increase is not really understood.

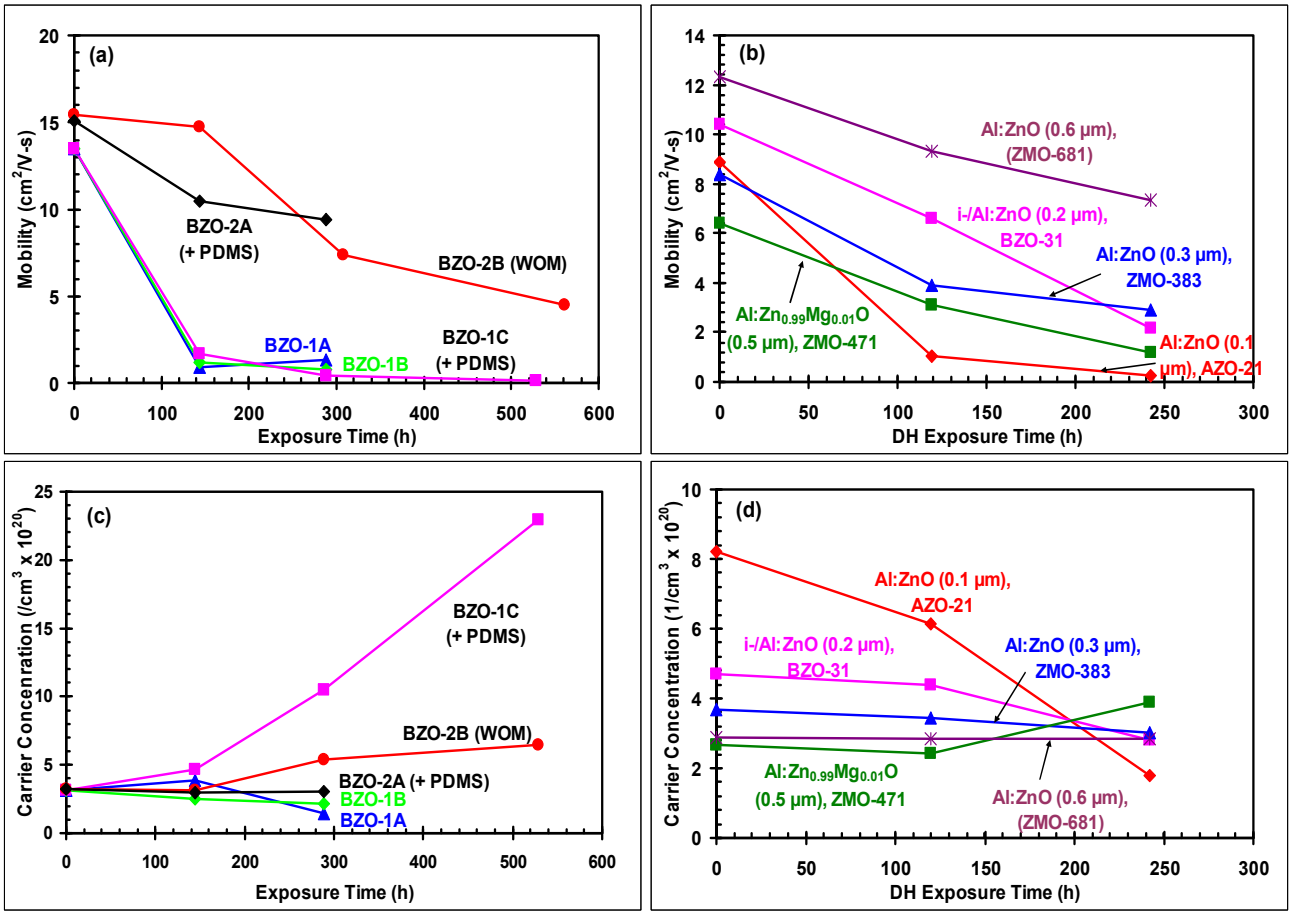

Fig. 5. Changes in (a and b) mobility and (c and d) carrier concentration for DH- and WOM-exposed ZnO and ZMO films. Curves for BZO films that were pretreated with PDMS are marked. All exposures, except that marked with WOM for weatherometer, were conducted in the damp heat chamber.

III. Structural Property and Degradation

As noted in Fig. 6, the majority of the ZnO films (IZO, AZO, and BZO) prepared on the Semicore system possessed a highly (002)-preferred orientation (Fig. 6c-f), however some BZO films studied in the first experiment showed considerably less (002) preference (Fig. 6b) and some were in between (Fig. 6a). The peaks at 2θ 38.12° and 44.45° in Fig. 6 (a and b) are tentatively assigned to be (201) and (211) with some uncertainty, even compared extensively to a number of PDF index cards for ZnO and Al_2O_3. The cause for these structural variations has not been investigated, but is probably due to some variations during sputtering. A similar strong (002) peak preference was also observed for the ZMO films (not shown). Figure 5 also shows the DH-induced changes in the XRD peak intensity and pattern, which are fairly irregular from one sample to another. This is particularly obvious for the (002) peak originally at 2θ 34.3°~34.5°, in which some films showed an early peak intensity increase (Fig. 6 (a and e)) and some showed a decrease (Fig. 6 (b, c, and f)), before exhibiting a moderate to large decrease at prolonged DH exposure due to structural disintegration. Except for the bilayer BZO-31 (Fig. 6f), all single-layer ZnO films showed an increase in (002) peak intensity up to DH 242 h. When rapidly degraded in the presence of acetic acid, the (002) peak in Fig. 6d almost completely disappeared, a clear indication of nearly total structural degeneration or destruction.

Red-shift of the (002) peak was also observed for BZO in Fig. 6 (c and f) and for IZO in Fig. 6e, suggesting a certain degree of change in the lattice. In addition, the peaks at 2θ 38.12° and 44.45° either disappeared (Fig. 6a) or largely decreased (Fig. 6b), suggesting a faster degradation of the corresponding ZnO structure. Additionally, the ZMO films

(ZMO-471 and ZMO-501 in Table 1) displayed unusual peak shifts. For example, the Al:$Zn_{0.9}Mg_{0.1}O$ (ZMO-501) alloy exhibited a main peak at 2θ 34.12° with a long tail (not shown) that shifted to ~33.95° upon DH exposure up to 242 h and then back to 34.12° at 480 h. More study is needed to further verify this behavior.

At DH = 480 h, the IZO-11 film in Fig. 6e and the Al:$Zn_{0.99}Mg_{0.01}O$ film (ZMO-471 in Table 1, XRD figure not shown) have four new peaks that appeared in the 2θ 31°–39° range, possibly a consequence of structural degeneration resulting from the hot moisture-induced degradation. The peaks at 31.38°, 33.22°, and 35.38° are assigned, using PDF#89-0510,

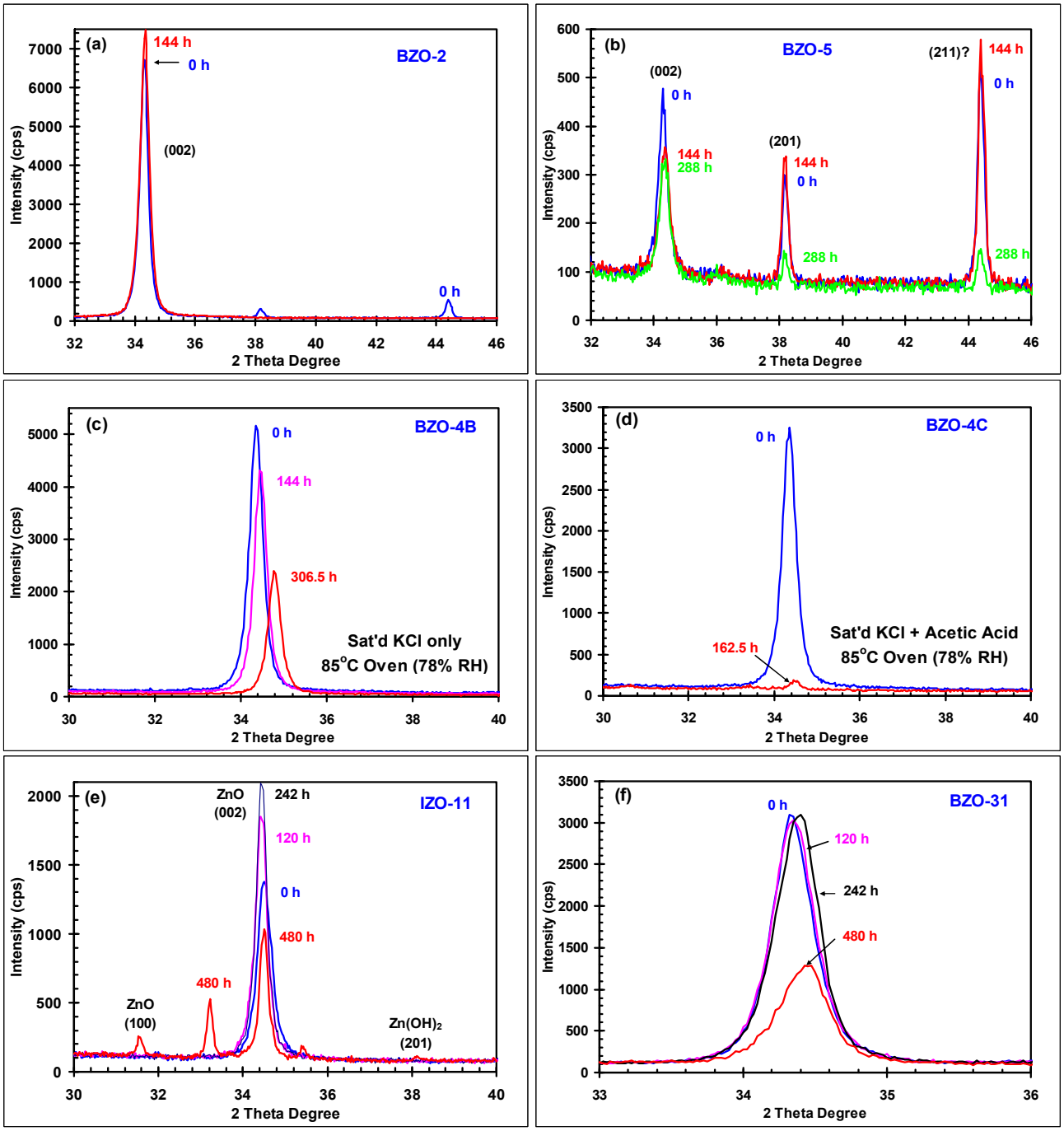

Fig. 6. X-ray diffractograms for (a, b, c, d, f) BZO films and (e) an IZO film upon damp heat exposures at 85°C and 85% RH, except for (c and d) as marked. The exposure times are indicated in each figure. Samples BZO-4 and 5 are not given in Table 1.

65-2880, and 75-1533 index references for ZnO, to be hexagonal (100), cubic (111), and hexagonal (101), respectively. The peak at 38.12° may be from cubic (200) or $Zn(OH)_2$ (201), as referred to PDF #65-2880 and 89-0138.

The observed XRD results are quite complicated and cannot be explained straightforwardly. However, coupled with SEM and optical micro-imaging results (see below), the (002) peak intensity increase in the early DH exposure may be explained by an increase in the film thickness and/or morphological changes. On the other hand, a decrease in (002) peak intensity in the early DH exposure may have resulted from early structural deterioration. However, the mechanism(s) that govern(s) such different structural changes is (are) not clear. Despite this perplexity, the XRD results in general suggest that the ZnO might have undergone structural degeneration from an original highly (002) preferential orientation to a more disordered state with some transformation from original hexagonal to cubic, in addition to the formation of insulating ZnO and $Zn(OH)_2$. Feist et al. also proposed the formation of $Zn(OH)_2$ to be the main cause of degraded CIGS mini-module performance upon DH treatment.[29] Meanwhile, it is not clear yet on the fate of the Al dopant upon DH exposure, although it is possible that the Al was also readily transformed into $Al(OH)_3$. The ZMO alloys probably also underwent similar hydrolysis and turned into a mixture $Zn(OH)_2$ and $Mg(OH)_2$.

IV. Morphological Degradation

IV-1. Optical Micro-Imaging

The ZnO and ZMO films were examined periodically during the course of DH exposures, in addition to the optical, electrical, and structural measurements described above, with optical micro-imaging using a WYKO interference microscope, which became available in the second experiment, for the initiation and propagation of the defecting patterns and regions as a function of DH exposure time. More than 1000 micro-images were taken. A few of the images are illustrated here. Figure 7 shows the progressive morphological degradation for the single-layer i-ZnO sample (IZO-11) at four stages, as the DH exposure time increased to 480 h. The initially grainy but fairly smooth surface started to show some small spikes that appeared in a random manner upon DH exposure in the first ~100 h. The number of spikes increased along with the appearance of full or partial ring-like features that showed ditch-like cutting into the depth of the film as the DH time increased (e.g., 240 h). The ring features are suspected to arise from the finite water droplets condensed from the moisture, which were observed when the cool films were just loaded into the hot steamy DH chamber. As the degradation progressed further, the film disintegrated greatly into fabric-like features at DH 480 h and was difficult to be micro-photographed because of large loss of light reflection from the rough surface. This morphological degradation process and pattern development was essentially the same for all ZnO-based films as observed in this study, as further illustrated in Fig. 8 for the single-layer AZO-21, bilayer BZO-31, and two ZMO films. The changing rate of the morphological images shows that bilayer BZO-31 at 0.2 μm degraded more slowly than the single-layer IZO-11 and AZO-21 at 0.1 μm, consistent with the electrical degradation rates given in Table 1. Similar surface morphological degradations were also observed for the two samples of $Al:Zn_{1-x}Mg_xO$ alloy at DH 242 h, as seen in Fig. 8 (bottom row). At 10% of MgO (x = 0.1), the $Al:Zn_{0.9}Mg_{0.1}O$ (ZMO-501) was originally insulating and, upon DH exposure, exhibited localized spot-wise material loss (see the second image from right of the bottom row), suggesting the MgO-ZnO was not fully alloyed in the co-sputtering process.

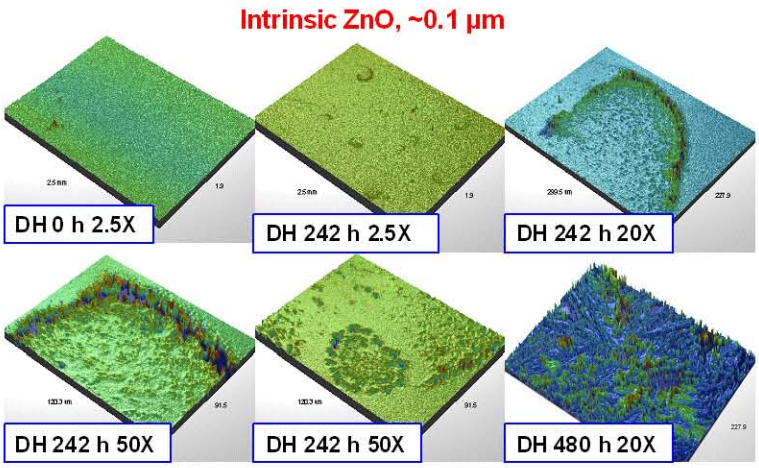

Fig. 7. Optical micro-images for the sample of intrinsic ZnO (IZO-11), showing the progressive morphological degradation as the DH exposure time increased to 480 h. The magnification factors are indicated.

These close observatons allow a generalization of the degrading process induced by the DH as follows. The first sign of degradation started at a few small spots or areas with the appearance of irregular circles and spikes (e.g., Figs. 7 and 8 at 120~242 h). As the DH exposure increased, the hydrolysis-induced corrosion circles, spikes, and pop-ups increased and became more widely spread (e.g., Figs. 7 and 8 at DH 242 h). Finally, especially for ZnO-based films, severe disintegration resulted (e.g., Fig. 7 at DH 480 h). This thermal hydrolytic process might have started from the surface of the film as well as at the grain boundary and progressed downward and inward. If this was the case, then it would take longer exposure time to allow the "ditches" (e.g., Figs. 7 and 8, leftmost figure at the bottom row) to grow deeper to break up the electrical conducting path on a thicker ZnO film, and to break up the better grain crystallites on a ZnO film made at higher temperature. In addition, visible delaminations were seen on some ZnO films after 480 h DH exposure, suggesting the destruction of the bonding at the interface between the ZnO layer and glass substrate.

IV-2. SEM Micro-Imaging

The ZnO and ZMO films before and after DH exposures were also subject to scanning electron microscopic analysis for changes in surface morphology and cross-sectional structures. Figure 9 (a and b columns) demonstrates the large morphological changes for the single-layer i-ZnO and Al:ZnO, and bi-layer i-/Al:ZnO before and after 480-h DH exposure. The originally smooth surfaces with very small grains seen at very high magnification at 200,000X became strangely featured. Furthermore, the obvious morphological differences in the Fig. 9 (b column) also suggest the three ZnO films had probably experienced different reaction rates/paths with the hot steam that resulted in different features or structures from the degradation products. More strikingly observed from the cross-sectional SEM analysis are porous formations of the DH-degraded films (Fig. 9), and segregation of the film materials into round zones (e.g., AZO-21, not shown), seem to correspond to the partial or full cycles with ditching features seen in the WYKO optical micro-images (Figs. 7 and 8). The segregation resulted in some (ditched) areas becoming very thin and the film materials within swelling and becoming very thick, as shown in Fig. 9 (c column, middle) for IZO-11. Finally, as revealed from the cross-section images, all three exposed ZnO films are five to ten times thicker than their originals, as a result of DH-induced degradation. The increase in film thickness as well as surface morphological roughness may explain the initial increase of the (002) peak intensity in XRD analysis. The porous formation may have also contributed to the thickness increase. The surface morphologies of the DH-exposed, single-layer ZMO films (ZMO-383, 471, and 501 in Table 1) made on the ATC 2200-V sputtering system also showed varying changes, but are not shown here.

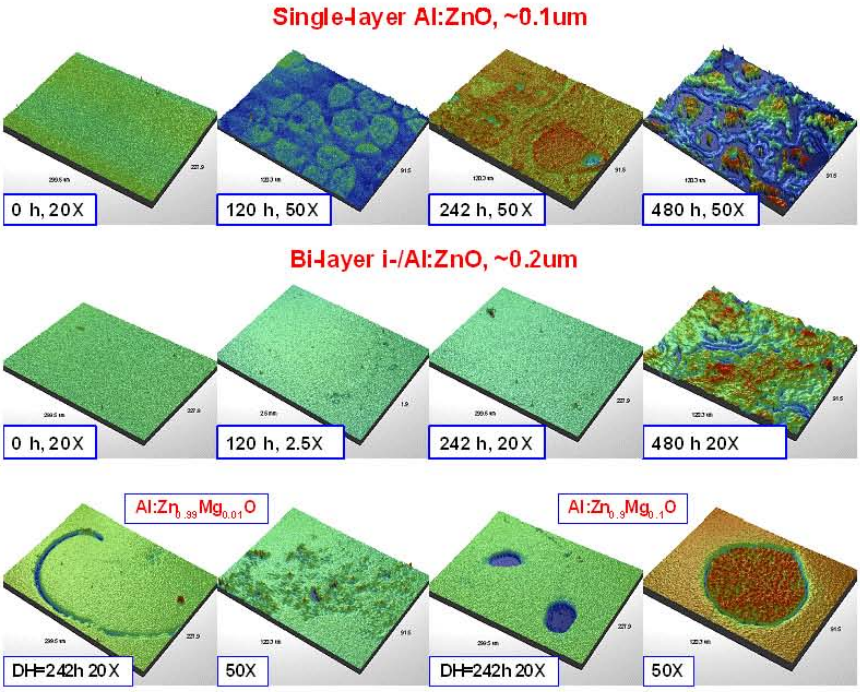

Fig. 8. Optical micro-images for the samples of (top row) single layer Al:ZnO (AZO-21), (middle row) bilayer i-/Al:ZnO (BZO-31), and (bottom row) Al:$Zn_{1-x}Mg_xO$, x = 0.01 and 0.1, (ZMO-471 and ZMO-501), showing morphological degradations at DH = 242 h or 480 h exposure. The magnification factors are indicated.

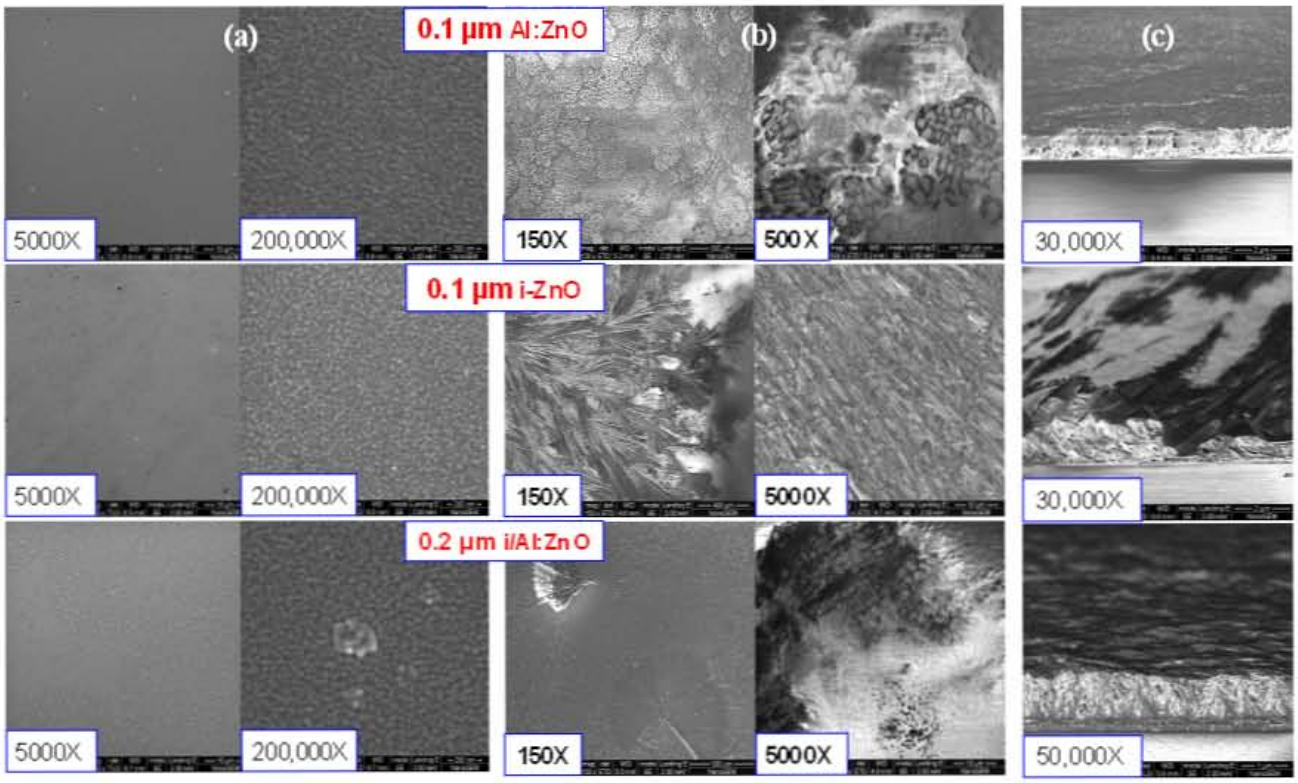

Fig. 9. SEM micrographs for (top row) single layer Al:ZnO (AZO-21), (middle tow) single-layer i-ZnO (IZO-11), and bilayer i-/Al:ZnO (BZO-31) showing topographs before (a column) and after (b column) DH = 480 h exposure. Images in the (c column) are for the cross-sections of the samples, taken with a 10^{o} tilt in view angle. The magnification factors are indicated.

V. Proposed Damp Heat-Induced Degradation Mechanism

As summarized from all observations of optical, electrical, structural, morphological changes induced by the accelerated DH exposures, the temporal process of DH-induced degradation is proposed to involve these steps:

1. First, hydrolysis of the oxides at some sporadic "weak" (defect) spots
2. Swelling and popping of the hydrolyzed spots due to volume increase
3. "Segregation" of hydrolyzed regions causing discontinuity of electrical path
4. Hydrolysis of the oxide-glass interface
5. Finally, formation of insulating metal hydroxide along with visible delamination over larger areas.

VI. Chemical and Physical Mitigations

Preliminary studies were conducted to investigate the feasibility of protecting the bilayer i-/Al:ZnO from DH degradation. The first was a chemical mitigation method that attempted to reduce the hydrophilicity of the ZnO by coating the surface, and perhaps the grain boundary too, with a hydrophobic silane that can form covalent bonding with the hydroxyl groups on the ZnO. PDMS, a widely used silane for surface coating, was tried in this study with limited success as discussed in Section II. An improvement in the treatment condition and silane solution formulation may improve the protective effect. Recently, Kim et al. reported that a simple coating of ZnO nanowires, which were very sensitive to ambient gas and humidity, with polymethylmethacrylate (PMMA) was useful to passivate the surface states on the nanowires and so reduce the moisture-induced degradation rate.[33]

The second was a physical mitigation method that deposited on the BZO surface a moisture-blocking silicon oxynitride (SiO_xN_y) by the PECVD method. The SiO_xN_y as a "barrier oxide" coating has been studied several years at NREL to block moisture vapor transmission through polymer films of the "back foils" for PV module encapsulation applications.[34,37,38] SiO_2 is another barrier oxide commonly used in multi-layer films by the packaging industry. Figure 10 shows the significant changes in transmittance and reflectance spectra of a BZO film upon coating with a thin layer (~0.4 μm) of SiO_xN_y. Whether the SiO_xN_y can be also used as antireflection coating, in addition to the physical protecting layer, remains to be investigated. Upon DH exposure, however, the SiO_xN_y coating layer was largely cracked, visibly flaked, and partially lost due to poor adhesion to the ZnO surface, and possibly internal stress also, as seen in the optical micro-images shown in Fig. 10. By chemically modifying the BZO surface, it is possible to improve the adhesion thereby reducing the stress of the SiO_xN_y. More work has been undertaken in the mitigation studies by improving the surface treatment conditions with silanes including PDMS for BZO and ZMO (with 2%-5% MgO) as well as for the SiO_xN_y coating layer.[39] Initial observations suggest that it is possible to improve the adhesion of SiO_xN_y coating on the BZO. Successful results will be reported in the near future.

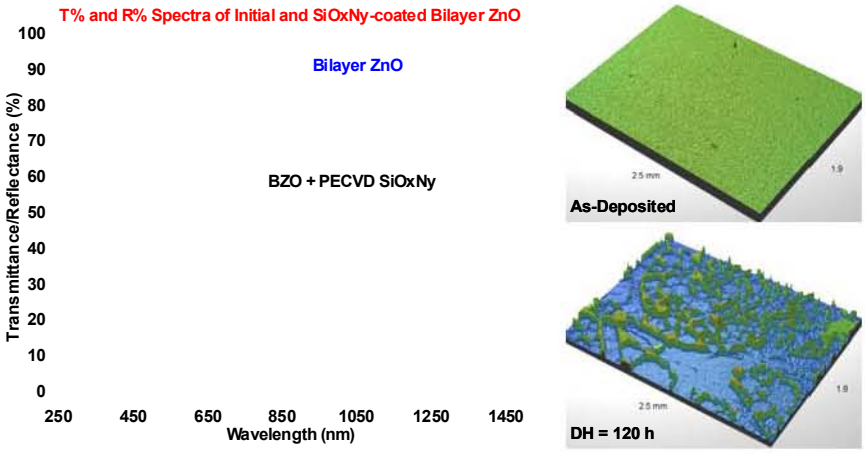

Fig. 10. (Left) Transmittance and reflectance spectra for a bilayer ZnO film before and after coating with a SiO_xN_y layer by PECVD, (right) optical micro-images for the SiO_xN_y–coated BZO before (top) and after (bottom) 120 h exposure in damp heat.

CONCLUSIONS

Accelerated exposure-induced degradation of single-layer and bilayer undoped and Al-doped ZnO and ZnMgO alloys for CIGS solar cells was investigated with optical, electrical, structural, and optical and SEM micro-imaging characterization. The results show that the degradation rate follows the trend of (damp heat in the presence of acetic acid) > (damp heat) > (in weatherometer). The degradation rate was also affected by film thickness, deposition substrate temperature, and periodic "dry-out." A temporal degradation mechanism for the ZnO films in damp heat was proposed with a structural transformation and/or degeneration from originally high (002) preference by hydrolysis into highly resistive $Zn(OH)_2$. Similar degradation consequences may be also true for the two ZMO alloys at 1% and 10% MgO in this study. Preliminary studies on chemical and physical mitigation methods were investigated. Limited success was observed for the chemical surface treatment using a hydrophobic PDMS. A physical mitigation method using a PECVD-SiO_xN_y coating on the bilayer ZnO failed in damp heat by poor adhesion. More ZMO alloys with 2%-5% MgO have been fabricated and their stability was recently investigated along with further studies on the mitigation methods.

ACKNOWLEDGEMENTS

We thank NCPV staff D. Albin for useful discussion, J. Zhou for some XRD measurements, J. Pankow for XPS analysis, and T. Gessert for manuscript review and discussion, respectively. This work was performed at the National Center for Photovoltaics under DOE contract number DE-AC36-99-GO10337 with the National Renewable Energy Laboratory.

REFERENCES

[1] Photon International, March, pp. 152, 2008.

[2] T. Minami, "New n-Type Transparent Conducting Oxides," MRS Bulletin, **25**, pp. 38-44, 2000.

[3] E. Fortunato, D. Ginley, H. Hosono, and D. C. Paine, "Transparent Conducting Oxides for Photovoltaics," MRS Bulletin, **32**, pp. 242-247, 2007.

[4] R. G. Gordon, "Criteria for Choosing Transparent Conductors," MRS Bulletin, **25**, pp. 52-57, 2000.

[5] M. A. Green, "Thin-Film Solar Cells: Review of Materials, Technologies and Commercial Status," J. Mater. Sci: Mater. Electron, **18**, S15-S19, 2007.

[6] R. W. Miles, G. Zoppi, and I. Forbes, "Inorganic Photovoltaic Cells," Materials Today, **10**, pp. 20-27, 2007.

[7] R. E.I. Schropp, R. Carius, and G. Beaucame, "Amorphous Silicon, Microcrystalline Silicon, and Thin-Film Polycrystalline Silicon Solar Cells," MRS Bulletin, **32**, pp. 219-224, 2007.

[8] (a) D. Domine, J. Bailat, J. Steinhauser, A. Shah, and C. Ballif, "Micromorph Solar Cell Optimization Using a ZnO Layer as Intermediate Reflector," *Proc. 30th IEEE PVSC*, pp. 1465- 1468, 2006. (b) D. Domine, J. Steinhauser, L. Feitknecht, A. Shah, and C. Ballif, "Effect of ZnO Layer as Intermediate Reflector in Micromorph Solar Cells," *Proc. 20th European PVSEC*, Barcelona, Spain, pp. 1600-1603, 2005.

[9] T. Minemoto, T. Mizuta, H. Takakura, and Y. Hamakawa, "Antireflective Coating Fabricated by Chemical Deposition of ZnO for Spherical Si Solar Cells," Solar Energy Materials & Solar Cells, **91**, pp. 191-194, 2007.

[10] P. Suri and R.M. Mehra, "Effect of electrolytes on the Photovoltaics Performance of a Hybrid Dye Sensitized ZnO Solar Cell," Solar Energy Materials & Solar Cells, **91**, pp. 518-524, 2007.

[11] K. Wang, J. Chen, W. Zhou, Y. Zhang, J. Pern, Y. Yan, and A. Mascarenhas, "Synthesis and Optical Properties of Type II Core/Shell Nanowire Array for Solar Cell Application," *Proc. 33th IEEE PVSC*, San Diego, CA, May 11-16, 2008.

[12] H.S. Ullal and B. von Roedern, "Thin Film CIGS and CdTe Photovoltaics Technologies: Commercialization, Critical Issues, and Applications," *Proc. 22nd European PVSEC*, Milan, Italy, Sept. 3-7, 2007. NREL/CP-520-42058.

[13] B. von Roedern, "How Do Buffer Layers Affect Solar Cell Performance and Solar Cell Stability," *Mat. Res. Soc. Symp. Proc*., **668,** H6.9.1-6, 2001.

[14] L. Schmidt-Mende and J. L. MacManus-Driscoll, "ZnO – Nanostructures, Defect, and Devices," Materials Today, **10**, pp. 40-48, 2007.

[15] Repins, M. Contreras, M. Romero, Y. Yan, W. Metzger, J. Li, S. Johnston, B. Egaas, C. DeHart, J. Scharf, B. E. McCandless, and R. Noufi, "Characterization Of 19.9%-Efficient CIGS Absorbers," *Proc. 33th IEEE PVSC*, San Diego, CA, May 11-16, 2008.

[16] X. Li, H. Ray, C. L. Perkins, and R. Noufi, "Aluminum Doping Effects on The $Zn_{1-x}Mg_xO$:Al Transparent Conducting Films Deposited by rf Sputtering," Symposium KK5.15, MRS 2008 Spring Meeting, San Francisco, CA, March 24-28, 2008.

[17] D. Schmid, M. Ruckh, and H.W. Schock, Solar Energy Materials and Solar Cells, **41/42**, pp. 281. 1996.

[18] S. Choopun, R.D. Vispute, W. Yang, R. P. Sharma, and T. Venkatesan, "Realization of Band Gap above 5.0 eV in Metastable Cubic-Phase $Mg_xZn_{1-x}O$ Films," Appl. Phys. Lett., **80**, pp. 1529, 2002.

[19] K. Matsubara, H. Tampo, H. Shibata, A. Yamada, P. Fons, K. Iwata, and S. Niki, "Band-gap Modified Al-doped $Zn_{1-x}Mg_xO$ Transparent Conducting Films Deposited by Pulsed Laser Deposition," Appl. Phys. Lett., **85**, pp.1374–1376, 2004.

[20] H. Ryoken, I. Sakagichi, T. Ohgaki, N. Ohashi, Y. Adachi, and H. Haneda, "Defect Structures in Undoped and Doped ZnO Films Studied by Solid State Diffusion," *Mat. Res. Soc. Symp. Proc.*, **829**, B2.23.1-6, 2005.

[21] K. Whitfield, "Practical Application of the Standard Qualification Test Sequences to New Thin-Film Products," presentation file, *33th IEEE PVSC*, San Diego, CA, May 11-16, 2008.

[22] J. Pern and R. Noufi, " An Investigation of Stability Issues of ZnO and Mo on Glass Substrates for CIGS Solar Cells upon Accelerated Weathering and Damp Heat Exposures," *Proc. DOE SETP Review Meeting*, Denver, CO., April 17-19, 2007.

[23] F. J. Pern, R. Noufi, X. Li, C. DeHart, and B. To, "Damp-Heat Induced Degradation of Transparent Conducting Oxides for Thin-Film Solar Cells," *Proc. 33th IEEE PVSC,* San Diego, CA, May 11-16, 2008.

[24] M. Bär, J. Reichardt, I. Sieber, A. Grimm, I. Kötschau, I. Lauermann, S. Sokoll, T.P. Niesen, M.C. Lux-Steiner, and Ch.-H. Fischer, "ZnO Layers Deposited by the Ion Layer Gas Reaction on Cu(In, Ga)(S, Se)$_2$ Thin Film Solar Cell Absorbers – Impact of 'Damp Heat' Conditions on the Layer Properties," Progr. Photovolt: Res. Appl. **15,** pp. 187–198, 2007.

[25] J. Klaer, R. Klenk, A. Boden, A. Neisser, C. Kaufmann, R. Scheer, H.-W. Schock, "Damp Heat Stability of Chalcopyrite Mini-Modules: Evaluation of Specific Test Structures," *Proc. 31st IEEE PVSC*, pp. 336-339, 2005.

[26] H. Stiebig, W. Reetz, C. Haase, T. Rapmann, and B. Rech, "Stability of Non-encapsulated Thin-Film Silicon Solar Cells in Damp Heat Tests," *Proc. 15th International PV Sci. & Eng. Conf. (PVSEC-15)*, Shanghai, China, pp. 561-562, 2005.

[27] W. Lin, R. Ma, J. Xue, and B. Kang, « RF Magnetron Sputtered ZnO :Al Thin Films on Glass Substrates : A Study of Damp Heat Stability on Their Optical and Electrical Properties," Solar Energy Materials and Solar Cells, **91**, pp. 1902-1905, 2007.

[28] S. Wiedeman, J. Britt, J. VanAlsburg, W. Stoss, U. Schoop, E. Kanto, S. Lundberg, "Scale-Up at Global Solar Energy using Roll-to-Roll Processes for Thin Film CIGS PV" and poster presentation, *Proc. DOE SETP Review Meeting*, Denver, CO., April 17-19, 2007.

[29] R. Feist, S. Rozeveld, M. Mushrush, R. Kaley, B. Lemon, J. Gerbi, B. Nichols, R. Nilsson, T. Richardson, S. Sprague, R. Tesch, S. Torka, C. Wood, S. Wu, S. Yeung, and M. T. Bernius, "Examination of Lifetime-Limiting Failure Mechanisms in CIGSS-based PV Minimodules under Environmental Stress," *Proc. 33th IEEE PVSC*, San Diego, CA, May 11-16, 2008.

[30] L. Olson, S. Kundu, M. Gross, and A. Joly, "Damp Heat Effects on CIGSS and CdTe Cells," *Proc. DOE SETP Review Meeting*, Denver, CO., April 17-19, 2007.

[31] L. Olson, M. E. Gross, and S. Kundu, "Properties of Encapsulated CIGS Cells in 85^{o}C/85%RH," *Proc. 33th IEEE PVSC*, San Diego, CA, May 11-16, 2008.

[32] Vitex Systems press release, "Vitex Systems Achieves Lifetime Record on Flexible Copper Indium Gallium Selenide Solar Cells," http://www.vitexsys.com/new/index.php?action=release-detail&PRID=33. June 12, 2008.

[33] D.-W. Kim, S.-H. Choi, H.-J. Ji, S. W. Kim, S. E. Moon, S. J. Park, and G.-T. Kim, "Degradation of ZnO Nanowire Devices under The Ambient Conditions," *Mat. Res. Soc. Symp. Proc.*, **1080**, 1080-O15-08, 2008.

[34] S. H. Glick, J. A. del Cueto, K. Terwilliger, G. Jorgensen, B. M. Keyes, L. M. Gedvilas, and F. J. Pern, "Silicon Oxynitride Thin Film Barriers for PV Packaging," Poster presentation, *Proc. DOE SETP Review Meeting*, Denver, CO, Nov. 7-10, 2005.

[35] R. Noufi, "High Efficiency CdTe and CIGS Thin Film Solar Cells: Highlights of The Technologies Challenges," presentation file, *2006 IEEE 4th World Conf. on PEC,* Waikoloa, Hawaii, May 7-12, 2006. (NREL/PR-520-39773)

[36] A. W. Czanderna and F. J. Pern, "Encapsulation of PV Modules using Ethylene Vinyl Acetate Copolymer as A Pottant: A Critical Review," Solar Energy Materials and Solar Cells, **43,** pp. 101-181, 1996.

[37] G. Jorgensen, K. Terwilliger, S. Glick, J. Pern, and T. McMahon, "Materials Testing for PV Module Encapsulation," *Proc. DOE SETP Program Review Meeting*, Denver, CO, March 24-26, 2003.

[38] G. J. Jorgensen, K. M. Terwilliger, J. A. DelCueto, S. H. Glick, M. D. Kempe, J. W. Pankow, F. J. Pern, T. J. McMahon, "Moisture Transport, Adhesion, and Corrosion Protection of PV Module Packaging Materials," Solar Energy Materials & Solar Cells*,* **90**, pp. 2739–2775, 2006.

[39] J. Pan, F. J. Pern, X. Li, S. H. Glick, and L. Kerr, unpublished work.

REPORT DOCUMENTATION PAGE

Form Approved
OMB No. 0704-0188

PLEASE DO NOT RETURN YOUR FORM TO THE ABOVE ORGANIZATION.

1. REPORT DATE *(DD-MM-YYYY)*	2. REPORT TYPE	3. DATES COVERED *(From - To)*
August 2008	Conference Paper	

4. TITLE AND SUBTITLE
Degradation of ZnO Window Layer for CIGS by Damp-Heat Exposure: Preprint

5a. CONTRACT NUMBER
DE-AC36-99-GO10337

5b. GRANT NUMBER

5c. PROGRAM ELEMENT NUMBER

6. AUTHOR(S)
F.J. Pern, R. Noufi, B. To, C. DeHart, X. Li, and S. H. Glick

5d. PROJECT NUMBER
NREL/CP-520-42792

5e. TASK NUMBER
PVB76701

5f. WORK UNIT NUMBER

7. PERFORMING ORGANIZATION NAME(S) AND ADDRESS(ES)
National Renewable Energy Laboratory
1617 Cole Blvd.
Golden, CO 80401-3393

8. PERFORMING ORGANIZATION REPORT NUMBER
NREL/CP-520-42792

9. SPONSORING/MONITORING AGENCY NAME(S) AND ADDRESS(ES)

10. SPONSOR/MONITOR'S ACRONYM(S)
NREL

11. SPONSORING/MONITORING AGENCY REPORT NUMBER

12. DISTRIBUTION AVAILABILITY STATEMENT
National Technical Information Service
U.S. Department of Commerce
5285 Port Royal Road
Springfield, VA 22161

13. SUPPLEMENTARY NOTES

14. ABSTRACT *(Maximum 200 Words)*
The reliability of ZnO-based window layer for CuInGaSe2 (CIGS) solar cells was investigated. Samples of RF magnetron-sputtered, single-layer intrinsic and Al-doped ZnO and their combined bilayer on glass substrates were exposed in a weatherometer (WOM) and damp heat (DH) conditions with or without acetic acid vapor. The Al-doped ZnO and ZMO films showed irreversible loss in the conducting properties, free carrier mobility, and characteristic absorption band feature after <500-h DH exposure, with the originally clear transparent films turned into white hazy insulating films and the degradation rate follows the trend of (DH + acetic acid) > DH > WOM. The degradation rate was also reduced by higher film thickness, higher deposition substrate temperature, and dry-out intervals. The results of X-ray diffraction analysis indicate that the ZnO-based films underwent structural degeneration by losing their highly (002) preferential orientation with possible transformation from hexagonal into cubic and formation of Zn(OH)2. Periodic optical micro-imaging observations suggested a temporal process that involves initial hydrolysis of the oxides at sporadic weak spots, swelling and popping of the hydrolyzed spots due to volume increase, segregation of hydrolyzed regions causing discontinuity of electrical path, hydrolysis of the oxide-glass interface, and finally, formation of insulating oxides/hydroxides with visible delamination over larger areas.

15. SUBJECT TERMS
PV; transparent conducting oxides; intrinsic and Al-doped ZnO; ZnMgO alloy; accelerated exposure; damp heat; weatherometer; degradation; CIGS; thin-film solar cell

16. SECURITY CLASSIFICATION OF:			17. LIMITATION OF ABSTRACT	18. NUMBER OF PAGES	19a. NAME OF RESPONSIBLE PERSON
a. REPORT	b. ABSTRACT	c. THIS PAGE			19b. TELEPHONE NUMBER (*Include area code*)
Unclassified	Unclassified	Unclassified	UL		